THE JOURNAL OF PHYSICAL CHEMISTRY C

Article

Cite This: J. Phys. Chem. C 2018, 122, 10476−10481

pubs.acs.org/JPCC

Mixed Ionic Liquid Improves Electrolyte Dynamics in Supercapacitors

Naresh C. Osti,*[,†,∥] Alejandro Gallegos,[‡,∥] Boris Dyatkin,[§,⊥] Jianzhong Wu,[‡] Yury Gogotsi,[§] and Eugene Mamontov*[,†]

[†]Neutron Scattering Division, Oak Ridge National Laboratory, P.O. Box 2008 MS6455, Oak Ridge, Tennessee 37831, United States

[‡]Department of Chemical and Environmental Engineering, University of California, 900 University Avenue, Riverside, California 92521, United States

[§]Department of Materials Science and Engineering, and A. J. Drexel Nanomaterials Institute, Drexel University, 3141 Chestnut Street, Philadelphia, Pennsylvania 19104, United States

Supporting Information

ABSTRACT: Well-tailored mixtures of distinct ionic liquids can act as optimal electrolytes that extend the operating electrochemical window and improve charge storage density in supercapacitors. Here, we explore two room-temperature ionic liquids, 1-ethyl-3-methylimidazolium bis(trifluoromethylsulfonyl)imide (EmimTFSI) and 1-ethyl-3-methylimidazolium tetrafluoroborate (EmimBF$_4$). We study their electric double-layer behavior in the neat state and as binary mixtures on the external surfaces of onion-like carbon electrodes using quasielastic neutron scattering (QENS) and classical density functional theory techniques. Computational results reveal that a mixture with 4:1 EmimTFSI/EmimBF$_4$ volume ratio displaces the larger [TFSI$^-$] anions with smaller [BF$_4^-$] ions, leading to an excess adsorption of [Emim$^+$] cations near the electrode surface. These findings are corroborated by the manifestation of nonuniform ion diffusivity change, complementing the description of structural modifications with changing composition, from QENS measurements. Molecular-level understanding of ion packing near electrodes provides insight for design of ionic liquid formulations that enhance the performance of electrochemical energy storage devices.

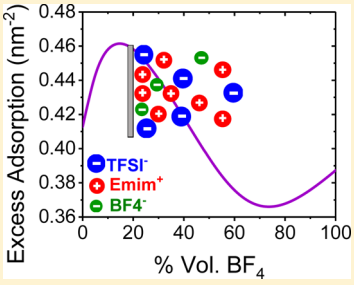

1. INTRODUCTION

Growing demand for electrical energy requires sustainable solutions that rely on renewable energy sources and efficiently store and release electrochemical energy.[1] Supercapacitors, which are also called ultracapacitors and electric double-layer capacitors (EDLCs), provide a balance between energy and power densities that allows them to charge at the same rate as traditional electrolytic capacitors and store charge at very high levels (>1 kW h/g).[2,3] To store charge, supercapacitors use electrosorption of electrolyte ions onto electrode surfaces under applied potentials. Their energy densities, which are determined by the total amount of stored charge and the stable operating voltage window, partially depend on the structure of the electrolyte−electrode interface and arrangement of ions in the electric double layer (EDL).[2] Because optimal energy densities can be directly attributed to the high accessible surface area of electrodes and minimal electrolyte breakdown under high potentials, many previous research efforts have tailored porous electrode architectures and matched them to the appropriate electrochemically stable electrolytes.[4−6]

Room-temperature ionic liquid (RTILs) electrolytes have gained particular attention owing their high electrochemical window, high thermal stability, low volatility, and molecular tunability.[7−9] Even though RTILs are less prone to electrochemical breakdown than other electrolytes,[10,11] their working operational voltage window (OPW) is still limited by the different electrochemical activities of anions and cations. Consequently, working potentials of the positive and negative electrodes in an EDLC are inherently asymmetric.[6,12] Various methods have attempted to address this asymmetry from an electrode perspective, for example, electrode mass balancing[6,13,14] and charge injection[12] into one or both electrodes. Different positive and negative electrode material compositions[15] have also been proposed. However, none of existing methods completely resolves the unbalanced charge distribution issue. Recently, an optimized binary mixture of two ionic liquids in a model system of onion-like carbon (OLC) electrodes has balanced charge storage with an increase in the OPW of the supercapacitor.[16] The mixture used ionic liquids with the same cation (1-ethyl-3-methylimidazolium or [Emim$^+$]) and two different anions (bis(trifluoromethylsulfonyl)imide or [TFSI$^-$] and tetrafluoroborate or [BF$_4^-$]). This balance on the capacitance of the electrodes shows that properties of the mixed electrolyte diverge from those of its constituents, and the OPW is extended from 2.5 to 3.5 V. However, fundamental molecular-level understanding of this beneficial mixing effect is still limited.

Mixing an ionic liquid with other ionic liquids[17,18] or co-solvents[19] alters its bulk properties such as diffusivity, viscosity, and electrical conductivity. Furthermore, a combination of several types of co-ions and counterions is expected to change

Received: March 15, 2018
Published: April 19, 2018

DOI: 10.1021/acs.jpcc.8b02521
J. Phys. Chem. C 2018, 122, 10476−10481

the resulting electrosorption densities on electrode surfaces. Recently, a classical density functional theory (cDFT) study on the EmimTFSI/EmimBF$_4$ mixtures has pinpointed an optimal 4:1 ratio mixture of the respective constituents that yields a maximum capacitance.[20] The effect was attributed to a significant reduction of the layering structures that enhanced the contact density of [Emim$^+$] counterions on the electrode surfaces because of the presence of smaller [BF$_4^-$] anions. However, a rational system design should rely on fundamental understanding that incorporates and rationalizes both the experimental[16] and computational results.[20]

Here, we examine the beneficial effect of mixing RTIL electrolytes for the most fundamental, basic system with zero applied potential. Interfacial phenomena involving various electrodes and electrolytes (aqueous and ionic liquids) have been explored using molecular dynamics simulations,[21] Monte Carlo simulations,[22,23] and cDFT.[24,25] Here, we utilize cDFT and quasi-elastic neutron scattering (QENS) to investigate the structure and microscopic dynamics of cations in the mixtures of EmimTFSI/EmimBF$_4$ adsorbed on the external surfaces of OLCs, which are concentric graphitic spheres of 5−10 nm in diameter.[26] We chose the OLC electrode model system because it facilitates a direct comparison of our findings against previous results, allows us to rely on a carbon structure that is commonly used in supercapacitors, and presents an optimal electrode−electrolyte interface that benefits from a high specific surface area (SSA) without convolution from internal confinement of ions. While they properly function as important model electrode systems, they are also useful in a number of commercial-scale applications. In addition to operating high-rate devices,[27] they act as substrates for grafted redox-active species and function as pseudocapacitors[28] and are integral for energy storage devices that operate under extreme temperature conditions.[29] Furthermore, other devices, such as micro-supercapacitors, benefit from the external surface area structures of OLCs.[30] We have found that a 4:1 v/v mixture of EmimTFSI/EmimBF$_4$ demonstrates the highest cation diffusivity and corresponds with peak adsorption of cations on the OLC surface. This experimental observation is further supported by the computed excess adsorption of the cation on the electrode surface. These findings, which match previously reported RTIL mixture compositions that had extended the OPW of supercapacitors,[16] reveal the microscopic dynamics of the cations in an ionic liquid mixture associated with the highest capacitance. Our findings provide further guidance for tuning electrolyte properties for electrochemical energy storage device design.

2. MATERIALS AND METHODS

2.1. Synthesis of Carbon Onions. OLCs were synthesized according to the previously established procedure.[31,32] UD-90 (Nanoblox, Inc.) nanocrystalline diamond powder (5−10 nm diameter particles) was placed into a graphite crucible and loaded into a vacuum furnace (Solar Atmospheres). The sample was outgassed for 24 h at 25 °C. The furnace reached a high vacuum (10^{-6} Torr) during this time. The furnace was ramped up to 1800 °C (at a rate of 10 °C min^{-1}), held at that temperature for 8 h, and cooled down to room temperature.[26] The process fully converted sp^3-bonded carbon in nano-diamond into concentric fullerene-type layers of sp^2-bonded graphitic carbon. The spherical structures exhibited only an external surface area (no internal porosity), and gas sorption measurements[33] found the OLC SSA to be 400 m^2 g^{-1} and its external pore volume to be 1.16 cm^3 g^{-1}.

2.2. Absorption of Ionic Liquids onto OLC Surfaces. RTILs and various mixtures were absorbed onto surfaces of OLCs according to the previously established vacuum infiltration procedure.[34−36] All ionic liquids were purchased from IoLiTec. Measured mass amounts of ionic liquids were dispersed in acetonitrile at room temperature (99.99% purity, Alpha Aesar) using magnetic stirring. This experiment investigated three different ionic liquid combinations: (1) pure EmimTFSI; (2) pure EmimBF$_4$; and (3) 80 vol % EmimTFSI/20 vol % EmimBF$_4$ mixture.[16] OLC powders were added to the solutions during stirring in ratios that would allow for the predetermined amounts of RTIL(s) to fully occupy the external pore volume of each OLC system. To determine the ratios, the bulk density of neat EmimTFSI was assumed to be 1.50 g cm^{-3}, and the bulk density of neat EmimBF$_4$ was assumed to be 1.25 g cm^{-3}. Three additional RTIL-only dispersions (without added OLC) were prepared with identical ratios stated above using the same dispersion and stirring method. The mixtures were continued to stir overnight until acetonitrile evaporated, and the resulting materials were dried for 24 h under a low vacuum (0.01 Torr) at 80 °C.

2.3. Loading into QENS Cans. The samples were placed into cylindrical annular and flat-plate aluminum cans for QENS experiments and sealed with indium wire. OLC-containing samples used flat-plate cans with 0.025 cm thick deep inserts, and RTIL-only samples used the annular cans with insets providing 0.005 cm thick samples to control the effects due to multiple scattering. All samples were sealed inside of an Ar-filled glovebox (Vacuum Atmospheres).

2.4. Classical Density Functional Theory. For this work, we employ the primitive model of electrolytes to represent RTILs. Although atomic details are lost in this model, it accounts for important characteristics including the ionic excluded volume and electrostatic correlation effects. Here, cations and anions are represented as charged hard spheres and the electrode surface is represented by a planar surface. The diameter of [Emim$^+$] is 0.50 nm, [BF$_4^-$] is 0.40 nm, and [TFSI$^-$] is 0.55 nm. The ion density in the bulk is fixed at 4.64 nm^{-3} for pure EmimTFSI and 7.78 nm^{-3} for pure EmimBF$_4$, corresponding to the ionic liquids at 298 K and 1 bar. The number density of the mixture can be reasonably assumed to be a linear combination between the two pure RTILs based off the volume of mixing for ionic liquids being very small (<0.1%).[37]

Within the primitive model, the pair potential (u_{ij}) between ionic species i and j is provided by a hard-core repulsion calculation plus Coulombic interaction

$$u_{ij}(r) = \begin{cases} \infty & r < \dfrac{\sigma_i + \sigma_j}{2} \\ \dfrac{Z_i Z_j e^2}{4\pi\varepsilon_0 \varepsilon r} & r \geq \dfrac{\sigma_i + \sigma_j}{2} \end{cases} \quad (1)$$

where r is the center-to-center distance, e is the unit charge, ε_0 is the permittivity of free space, and σ and Z are the diameter and valence, respectively, of each specific species. Because all ionic species are accounted for explicitly in this work, the relative dielectric permittivity is set to that of a vacuum ($\varepsilon = 1$).

The electrode is modeled as a planar wall, which has been shown to be an effective representation of an OLC.[20] The charged wall exerts an external potential on each ion given by

DOI: 10.1021/acs.jpcc.8b02521
J. Phys. Chem. C 2018, 122, 10476−10481

$$\beta V_i^{\text{ext}}(z) = \begin{cases} \infty & z < \frac{\sigma_i}{2} \\ -2\pi l_B Z_i Q z/e & z \geq \frac{\sigma_i}{2} \end{cases} \quad (2)$$

where z is the perpendicular distance from the wall, $\beta = 1/(k_B T)$, k_B is the Boltzmann constant, T is the temperature, $l_B = \beta e^2/(4\pi\varepsilon_0\varepsilon)$ denotes the Bjerrum length, and Q represents the surface charge density. Throughout this work, the Bjerrum length is taken to be 55.69 nm, corresponding to electrostatic interactions in a vacuum at room temperature.

To determine the density profiles of ionic species near the planar surface, we use cDFT. For a given temperature (T) and the bulk ionic density (ρ_i^b), the density profile for each species (i) is given by

$$\rho_i(z) = \rho_i^b \exp[-\beta V_i^{\text{ext}}(z) - \beta Z_i e\psi(z) - \beta\Delta\mu_i^{\text{ex}}(z)] \quad (3)$$

where $V_i^{\text{ext}}(z)$ is the nonelectrostatic component of the external potential as given by eq 2 and $\Delta\mu_i^{\text{ex}}(z)$ is the excess chemical potential which accounts for the thermodynamic nonideality due to the electrostatic correlations and excluded volume effects. The electrostatic part of the external potential is accounted for in the overall local electrical potential, $\psi(z)$, which is related to the local charge density by the Poisson equation

$$\frac{\partial^2\psi(z)}{\partial z^2} = -\frac{e}{\varepsilon_0}\sum_i Z_i\rho_i(z) \quad (4)$$

Equations 3 and 4 are solved self-consistently with the boundary conditions for the electrical potential

$$\psi(0) = \psi; \qquad \psi(\infty) = 0 \quad (5)$$

In the cDFT calculations, the electrical potential at the electrode surface, ψ, is assumed to be constant and for this work, is set to zero to represent an electrode with no applied potential. The excess ion adsorption is given by

$$\Gamma^{\text{ex}} = \int dz[\rho(z) - \rho^b] \quad (6)$$

2.5. QENS Measurement. Dynamics of cations in the samples were measured using the backscattering spectrometer (BASIS)[38] at the Spallation Neutron Source, Oak Ridge National Laboratory. BASIS is a time-of-flight inverted geometry spectrometer that provides a fine energy resolution of 3.5 μeV (at full width at half maximum) while using Si(111) analyzer crystals covering Q-space of 0.20−2.0 Å^{-1}. Data within the energy transfer range of ±100 μeV were analyzed. The sample temperature was controlled by a standard top-loading closed-cycle refrigerator. Sample-specific resolution at ∼20 K was measured from each sample. Elastic scan was performed from 20 to 300 K at 2 K increment. QENS data were collected at 300 K from each sample.

3. RESULTS AND DISCUSSION

Earlier electrochemical and cDFT studies[16,20] have identified a volcano-shaped correlation between capacitance and the fraction of $EmimBF_4$ in a mixture with EmimTFSI under applied potential, with a maximum at a 20% concentration. Our initial goal was to investigate the fundamental behavior of ions for different binary RTIL mixture concentrations adsorbed on the same external OLC surfaces as used in the previous studies. The primary objective of this effort was to determine whether the volcano-shaped trend of the capacitance observed at the applied potential translates into discernible dynamics under ambient conditions. To investigate this, we utilize cDFT because it has already been shown to properly capture the experimental findings on the capacitance trend with ionic liquid mixtures.[20] The details on the theoretical model and method are presented in section 2. Figure 1 shows the cDFT-derived

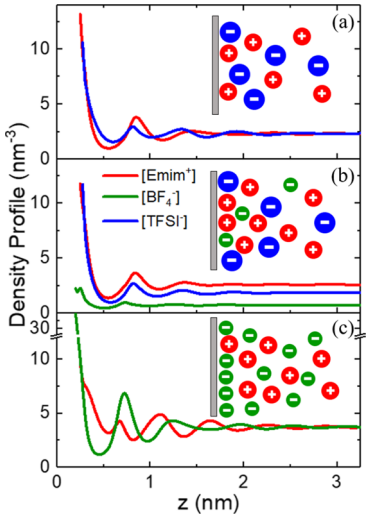

Figure 1. Ion distribution for cations and anions in EDLCs of pure and mixed EmimTFSI/$EmimBF_4$ ionic liquids near a surface with no applied potential as predicted by cDFT: (a) 0, (b) 13, and (c) 100 vol % $EmimBF_4$. The insets show a schematic of the EDL structure.

density profiles of cations and anions for pure EmimTFSI, pure $EmimBF_4$, and the 80:20 by mol % (87:13 by vol %) binary mixture of the two RTILs adsorbed on the surface of an OLC electrode with no applied potential. In the case of pure EmimTFSI (Figure 1a), the ionic density profiles are similar because of the similarity in size between the [$Emim^+$] cation and [$TFSI^-$] anion. However, because [$Emim^+$] is slightly smaller in size, the cations dominate the adsorption and induce a small negative surface charge on the electrode. In contrast to pure EmimTFSI, pure $EmimBF_4$ (Figure 1b) is more strongly affected by a substantial difference in size between the cation and anion. Because [BF_4^-] is smaller than [$Emim^+$], the anion is prevalent in the electrode−electrolyte interface and induces a large positive charge on the electrode.

When BF_4 is introduced into pure EmimTFSI, the large anion [$TFSI^-$] is replaced by the small anion [BF_4^-]. The stronger electrostatic interaction between [$Emim^+$] and [BF_4^-] as well as the reduced volume taken by the anions near the wall allows the cations to fill this available space.

Figure 2 shows the excess [$Emim^+$] adsorption as given by eq 6 within 0.93 nm of the wall. Here, it can be clearly seen that the excess [$Emim^+$] adsorption exhibits a maximum with 13 vol % concentration of [BF_4^-]. In agreement with previous results, the smaller anion displaces the larger cation and, in turn, forces it to occupy the now-available space in the diffuse layer near the OLC layer immediately outside of the direct OLC−electrolyte interface. This arrangement of [$Emim^+$] benefits from increased electrostatic attraction to the smaller [BF_4^-]. Interestingly, the excess [$Emim^+$] concentration also shows a minimum at 75 vol % $EmimBF_4$ concentration. However, contrary to the origin of the maximum, this minimum is a result of the introduction of

DOI: 10.1021/acs.jpcc.8b02521
J. Phys. Chem. C 2018, 122, 10476−10481

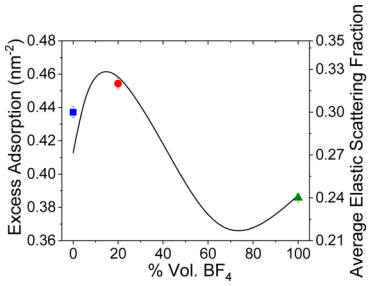

Figure 2. Excess adsorption of [Emim$^+$] near an OLC with no applied potential for pure EmimTFSI and EmimBF_4 and their mixtures as predicted by cDFT (left *y*-axis). The excess adsorption is given by $\Gamma^{ex} = \int dz[\rho(z) - \rho^b]$. Experimentally measured average elastic scattering fraction at three different EmimBF4 compositions is also shown (right *y*-axis).

the large [TFSI$^-$] into the system. This ion displaces cations from the wall and decreases overall number of cations due to a weaker electrostatic attraction and preferential adsorption of [TFSI$^-$] to the electrode interface that induces a net positive charge.

To understand the impact on the microscopic dynamics of the structural modifications in the adsorbed ions with changing composition as predicted from cDFT, we carried out QENS experiment to examine the microscopic cation dynamics in pure EmimTFSI and EmimBF_4 and their mixtures near OLC surfaces under no applied potential using a neutron backscattering spectrometer.[38] A very high incoherent neutron scattering cross section of hydrogen[39] makes QENS a method of choice to study the dynamics of fluids such as water and ionic liquids in bulk as well as in confinement.[34,40−42] Because the studied RTILs only feature hydrogen on [Emim$^+$] cations, the QENS spectra predominantly represent the contribution from cations of the ionic liquids. Analysis of the data (see Supporting Information for details) gives the diffusivity of cations from the *Q* (momentum transfer) dependence of quasi-elastic line width. Furthermore, the ratio of the elastic intensities to the total scattering intensities (elastic plus quasi-elastic) provides a measure of the amount of cations that are immobile and mobile (on ~10^{-9} s time scale defined by the QENS energy resolution).[43] Therefore, the elastic scattering fraction in the QENS spectra, which reflects the number of cations adsorbed on the electrode surface, should correlate with the computed excess adsorption of [Emim$^+$] near an OLC, which is indeed the case, as shown by the colored symbols in Figure 2.

We performed our measurements at zero applied potential to probe fundamental dynamics and properly complement cDFT results with the experimental findings. At first, we performed a temperature-dependent elastic scattering intensity measurement, from 20 to 300 K, with a 2 K increment. The normalized elastic scan (Figure S1 in Supporting Information) is qualitatively similar for all bulk-state reference samples, with a sharp decrease in intensity at higher temperatures due to electrolyte melting. Regardless of the variation in the melting temperature, the QENS spectra are similar among all samples at 300 K. A two-component model fit, which has been successfully used to extract the diffusivities of ionic liquids in bulk and in mixtures with cosolvents,[19,44,45] was adapted to probe the dynamics of cations. Half width at half-maximum (hwhm) of the model fit demonstrated a jump-type diffusion of the cations in all samples. Diffusion coefficients of [Emim$^+$] extracted using jump diffusion model are roughly the same (Figure in S2 in Supporting Information) at various concentrations (0, 20, and 100 vol %) of the [BF_4^-] ions in bulk liquids. Thus, irrespective of the size of the anions, the cation mobility is insensitive to variations in the composition in the bulk liquids.

Then, we performed elastic scattering intensity temperature scans of EmimTFSI and EmimBF_4 mixtures (0, 20, and 100 vol % of the [BF_4^-] ions) adsorbed on the surfaces of OLCs. Absence of abrupt changes in the elastic scan (Figure S3) that would be associated with melting indicates that all ionic liquids, whether in pure or mixed form, are completely confined inside the OLCs. The inset in Figure 3a depicts typical QENS spectra

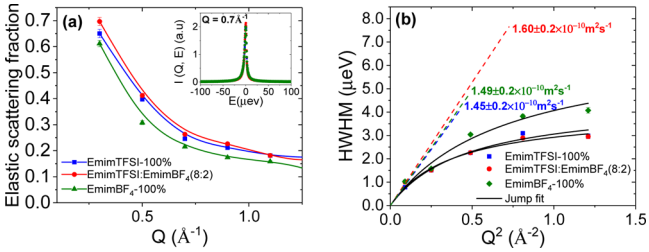

Figure 3. (a) Elastic scattering fraction obtained from the QENS spectra analysis using the model function described in the text. The inset shows representative QENS spectra. (b) Dependence of hwhm of a Lorentzian with Q^2. The solid lines are jump diffusion fits. The corresponding diffusivity values are also shown.

at 300 K from the confined ionic liquid mixtures and shows a higher scattering intensity at the elastic line from the mixture containing 20% of [BF_4^-] ions. This observation is quantified by the data presented in the main panel of Figure 3a, which indeed show systematical compositional dependence of the elastic scattering fraction. The *Q*-averaged data from Figure 3a presented with symbols in Figure 2 show the maximum excess adsorption of [Emim$^+$] near an OLC in the mixture of ionic liquids compared to the neat liquids. This result corroborates the cDFT prediction (solid line in Figure 2) for the excess adsorption of [Emim$^+$] on the surface of the electrodes.

The QENS spectra from the confined ionic liquids were further analyzed using an elastic scattering signal plus a sum of two Lorentzian functions (details in Supporting Information), each accounting for slower and faster processes, respectively. The slower process accounts for the long-range diffusivity of the cation, whereas the faster process is representative of a set of spatially localized motions.[44] Figure 3b presents hwhm of the narrow QENS component obtained from the model fit. The dependence of hwhm on Q^2 is not linear but instead characteristic of translational jump diffusion[46] of the cation. The diffusion coefficient obtained from the jump diffusion model fit is higher ($1.60 \pm 0.2 \times 10^{-10}$ m^2 s^{-1}) for the cation in the ionic liquid mixture containing 20 vol % of [BF_4^-] compared to the pure ionic liquids ($1.45 \pm 0.2 \times 10^{-10}$ m^2 s^{-1} in bulk EmimTFSI and $1.49 \pm 0.2 \times 10^{-10}$ m^2 s^{-1} in bulk EmimBF_4). Thus, Figure 3b shows the higher cation mobility in the ionic liquid mixture. This stems from the attachment of the larger number of cations to the OLC surface, in agreement with the cDFT computation. Such an arrangement leaves more room for the mobile cations away from the electrode−electrolyte interface, which, therefore, exhibit a higher diffusivity, as has previously been observed in confined ionic liquid systems.[44] Note that the broad component (Figure S4 in Supporting Information) demonstrates the presence of spatially

DOI: 10.1021/acs.jpcc.8b02521
J. Phys. Chem. C 2018, 122, 10476−10481

localized cation motion from the finite value of hwhm in the limit of $Q = 0$. Even though the hwhms of the broad component do not show any specific trend for the entire Q range, the higher values of the hwhms at low Q suggest the higher localized mobility (besides the higher long-range translational mobility) of the cation in the mixture.

Our results highlight the intricate behavior of ions that adsorb on the electrode surface and the effects of the dense initial layer and complementary diffusion layer on ion dynamics and electrosorption. Even under neutral potentials, ions do not behave like bulk ionic liquids at the electrode−electrolyte interfaces. These results agree with prior spectroelectrochemistry findings, which highlighted the fact that short-range rearrangement of ions, rather than bulk fluid flow, dominates electrolyte dynamics.[47] This behavior is present in every supercapacitor system and depends on the aspect ratio and external surface area of the carbon electrode confinement, and the mechanisms of ion dynamics in it are very important. These dynamics will become even more dominant in thin-film devices composed of two-dimensional materials.

4. CONCLUSIONS

In summary, cation diffusivity does not depend on the EmimTFSI/$EmimBF_4$ mixture composition in bulk liquid samples but shows a maximum for a 4:1 volume ratio of EmimTFSI to $EmimBF_4$ when the liquids are adsorbed on the surfaces of OLCs. This effect is due to the attachment of a larger number of cations to the interface of OLCs, which leaves more space in the immediate outer diffuse layer for mobile cations. This observation is supported by cDFT calculations that demonstrate a maximum excess adsorption of [$Emim^+$] for the same binary RTIL mixture composition. Our findings rationalize the observed volcano-shaped trend of the capacitance at the optimal relative ratio of the two ionic liquids. Because our experiments and modeling were conducted at zero applied potential, the concentration versus capacitance trend must be a general manifestation of the interplay between the ion size and charge near electrode surfaces, regardless of ambient or dynamic electrochemical conditions. Future efforts will probe the microscopic dynamics in the presence of an electromotive force, which is expected to further enhance the mobilities of the cations in the diffuse layer and yield the maximum integral capacitance predicted from cDFT. These findings provide a guidance to design electrolyte systems with optimized properties that will enhance energy and power densities of supercapacitors.

■ ASSOCIATED CONTENT

Supporting Information

The Supporting Information is available free of charge on the ACS Publications website at DOI: 10.1021/acs.jpcc.8b02521.

QENS data analysis and supporting QENS data (PDF)

■ AUTHOR INFORMATION

Corresponding Authors

*E-mail: ostinc@ornl.gov (N.C.O.).
*E-mail: mamontove@ornl.gov (E.M.).

ORCID

Naresh C. Osti: 0000-0002-0213-2299
Boris Dyatkin: 0000-0001-7537-2181
Jianzhong Wu: 0000-0002-4582-5941
Yury Gogotsi: 0000-0001-9423-4032
Eugene Mamontov: 0000-0002-5684-2675

Present Address

[⊥]U.S. Naval Research Laboratory, Washington, DC 20375, USA.

Author Contributions

[∥]N.C.O. and A.G. contributed equally.

Notes

The authors declare no competing financial interest.

■ ACKNOWLEDGMENTS

This work was supported as part of the Fluid Interface Reactions, Structures and Transport (FIRST) Center, an Energy Frontier Research Center funded by the U.S. Department of Energy, Office of Science, Office of Basic Energy Sciences. Work at ORNL's Spallation Neutron Source was sponsored by the Scientific User Facilities Division, Office of Basic Energy Sciences, U.S. Department of Energy. Oak Ridge National Laboratory is managed by UT-Battelle, LLC, for U.S. DOE under contract no. DEAC05-00OR22725. This research used resources of the National Energy Research Scientific Computing Center, a DOE Office of Science User Facility supported by the Office of Science of the U.S. Department of Energy under contract no. DE-AC02-05CH11231.

■ REFERENCES

(1) Larcher, D.; Tarascon, J.-M. Towards Greener and More Sustainable Batteries for Electrical Energy Storage. *Nat. Chem.* **2015**, *7*, 19−29.
(2) Simon, P.; Gogotsi, Y. Materials for Electrochemical Capacitors. *Nat. Mater.* **2008**, *7*, 845−854.
(3) Wang, G.; Zhang, L.; Zhang, J. A Review of Electrode Materials for Electrochemical Supercapacitors. *Chem. Soc. Rev.* **2012**, *41*, 797−828.
(4) Zhu, Y.; Murali, S.; Stoller, M. D.; Ganesh, K. J.; Cai, W.; Ferreira, P. J.; Pirkle, A.; Wallace, R. M.; Cychosz, K. A.; Thommes, M.; Su, D.; Stach, E. A.; Ruoff, R. S. Carbon-Based Supercapacitors Produced by Activation of Graphene. *Science* **2011**, *332*, 1537−1541.
(5) Simon, P.; Gogotsi, Y. Capacitive Energy Storage in Nanostructured Carbon-Electrolyte Systems. *Acc. Chem. Res.* **2013**, *46*, 1094−1103.
(6) Béguin, F.; Presser, V.; Balducci, A.; Frackowiak, E. Carbons and Electrolytes for Advanced Supercapacitors. *Adv. Mater.* **2014**, *26*, 2219−2251.
(7) Galiński, M.; Lewandowski, A.; Stępniak, I. Ionic Liquids as Electrolytes. *Electrochim. Acta* **2006**, *51*, 5567−5580.
(8) Armand, M.; Endres, F.; MacFarlane, D. R.; Ohno, H.; Scrosati, B. Ionic-Liquid Materials for the Electrochemical Challenges of the Future. *Nat. Mater.* **2009**, *8*, 621−629.
(9) Wishart, J. F. Energy Applications of Ionic Liquids. *Energy Environ. Sci.* **2009**, *2*, 956−961.
(10) Borges, R. S.; Ribeiro, H.; Lavall, R. L.; Silva, G. G. Temperature Stable Supercapacitors Based on Ionic Liquid and Mixed Functionalized Carbon Nanomaterials. *J. Solid State Electrochem.* **2012**, *16*, 3573−3580.
(11) Lin, Z.; Taberna, P.-L.; Simon, P. Graphene-Based Supercapacitors Using Eutectic Ionic Liquid Mixture Electrolyte. *Electrochim. Acta* **2016**, *206*, 446−451.
(12) Weng, Z.; Li, F.; Wang, D.-W.; Wen, L.; Cheng, H.-M. Controlled Electrochemical Charge Injection to Maximize the Energy Density of Supercapacitors. *Angew. Chem., Int. Ed.* **2013**, *52*, 3722−3725.

DOI: 10.1021/acs.jpcc.8b02521
J. Phys. Chem. C 2018, 122, 10476−10481

(13) Demarconnay, L.; Raymundo-Piñero, E.; Béguin, F. Adjustment of Electrodes Potential Window in an Asymmetric Carbon/MnO_2 Supercapacitor. *J. Power Sources* **2011**, *196*, 580−586.
(14) Vaquero, S.; Palma, J.; Anderson, M.; Marcilla, R. Improving Performance of Electric Double Layer Capacitors with a Mixture of Ionic Liquid and Acetonitrile as the Electrolyte by Using Mass-Balancing Carbon Electrodes. *J. Electrochem. Soc.* **2013**, *160*, A2064−A2069.
(15) Khomenko, V.; Raymundo-Piñero, E.; Béguin, F. A New Type of High Energy Asymmetric Capacitor with Nanoporous Carbon Electrodes in Aqueous Electrolyte. *J. Power Sources* **2010**, *195*, 4234−4241.
(16) Van Aken, K. L.; Beidaghi, M.; Gogotsi, Y. Formulation of Ionic-Liquid Electrolyte to Expand the Voltage Window of Supercapacitors. *Angew. Chem.* **2015**, *127*, 4888−4891.
(17) Fillion, J. J.; Brennecke, J. F. Viscosity of Ionic Liquid-Ionic Liquid Mixtures. *J. Chem. Eng. Data* **2017**, *62*, 1884−1901.
(18) Russina, O.; Lo Celso, F.; Plechkova, N. V.; Triolo, A. Emerging Evidences of Mesoscopic-Scale Complexity in Neat Ionic Liquids and Their Mixtures. *J. Phys. Chem. Lett.* **2017**, *8*, 1197−1204.
(19) Osti, N. C.; Van Aken, K. L.; Thompson, M. W.; Tiet, F.; Jiang, D.-E.; Cummings, P. T.; Gogotsi, Y.; Mamontov, E. Solvent Polarity Governs Ion Interactions and Transport in a Solvated Room-Temperature Ionic Liquid. *J. Phys. Chem. Lett.* **2017**, *8*, 167−171.
(20) Lian, C.; Liu, K.; Van Aken, K. L.; Gogotsi, Y.; Wesolowski, D. J.; Liu, H. L.; Jiang, D. E.; Wu, J. Z. Enhancing the Capacitive Performance of Electric Double-Layer Capacitors with Ionic Liquid Mixtures. *ACS Energy Lett.* **2016**, *1*, 21−26.
(21) Merlet, C.; Limmer, D. T.; Salanne, M.; van Roij, R.; Madden, P. A.; Chandler, D.; Rotenberg, B. The Electric Double Layer Has a Life of Its Own. *J. Phys. Chem. C* **2014**, *118*, 18291−18298.
(22) Bratko, D.; Henderson, D. J.; Blum, L. Limiting Law for Ion Adsorption in Narrow Planar Pores. *Phys. Rev. A: At., Mol., Opt. Phys.* **1991**, *44*, 8235−8241.
(23) Bhuiyan, L. B.; Bratko, D.; Outhwaite, C. W. Electrolyte Surface-Tension in the Modified Poisson-Boltzmann Approximation. *J. Phys. Chem.* **1991**, *95*, 336−340.
(24) Henderson, D.; Lamperski, S.; Jin, Z.; Wu, J. Density Functional Study of the Electric Double Layer Formed by a High Density Electrolyte. *J. Phys. Chem. B* **2011**, *115*, 12911−12914.
(25) Wu, J.; Jiang, T.; Jiang, D.-E.; Jin, Z.; Henderson, D. A Classical Density Functional Theory for Interfacial Layering of Ionic Liquids. *Soft Matter* **2011**, *7*, 11222−11231.
(26) McDonough, J. K.; Gogotsi, Y. Carbon Onions: Synthesis and Electrochemical Applications. *Interface* **2013**, *22*, 61−66.
(27) Miller, J. R.; Simon, P. Fundamentals of Electrochemical Capacitor Design and Operation. *Electrochem. Soc. Interface* **2008**, *17*, 31−32.
(28) Wang, Y.; Yu, S. F.; Sun, C. Y.; Zhu, T. J.; Yang, H. Y. MnO_2/Onion-Like Carbon Nanocomposites for Pseudocapacitors. *J. Mater. Chem.* **2012**, *22*, 17584−17588.
(29) Tsai, W.-Y.; Lin, R.; Murali, S.; Zhang, L. L.; McDonough, J. K.; Ruoff, R. S.; Taberna, P.-L.; Gogotsi, Y.; Simon, P. Outstanding Performance of Activated Graphene Based Supercapacitors in Ionic Liquid Electrolyte from-50 to 80 Degrees C. *Nano Energy* **2013**, *2*, 403−411.
(30) Huang, P.; Pech, D.; Lin, R.; McDonough, J. K.; Brunet, M.; Taberna, P.-L.; Gogotsi, Y.; Simon, P. On-Chip Micro-Supercapacitors for Operation in a Wide Temperature Range. *Electrochem. Commun.* **2013**, *36*, 53−56.
(31) McDonough, J. K.; Frolov, A. I.; Presser, V.; Niu, J.; Miller, C. H.; Ubieto, T.; Fedorov, M. V.; Gogotsi, Y. Influence of the Structure of Carbon Onions on Their Electrochemical Performance in Supercapacitor Electrodes. *Carbon* **2012**, *50*, 3298−3309.
(32) Weingarth, D.; Zeiger, M.; Jäckel, N.; Aslan, M.; Feng, G.; Presser, V. Graphitization as a Universal Tool to Tailor the Potential-Dependent Capacitance of Carbon Supercapacitors. *Adv. Eng. Mater.* **2014**, *4*, 1400316.
(33) Baturina, O.; Lu, Q.; Xu, F.; Purdy, A.; Dyatkin, B.; Sang, X.; Unocic, R.; Brintlinger, T.; Gogotsi, Y. Effect of Nanostructured Carbon Support on Copper Electrocatalytic Activity toward CO_2 Electroreduction to Hydrocarbon Fuels. *Catal. Today* **2017**, *288*, 2−10.
(34) Dyatkin, B.; Osti, N. C.; Zhang, Y.; Wang, H.-W.; Mamontov, E.; Heller, W. T.; Zhang, P.; Rother, G.; Cummings, P. T.; Wesolowski, D. J.; Gogotsi, Y. Ionic liquid structure, dynamics, and electrosorption in carbon electrodes with bimodal pores and heterogeneous surfaces. *Carbon* **2018**, *129*, 104−118.
(35) Dyatkin, B.; Zhang, Y.; Mamontov, E.; Kolesnikov, A. I.; Cheng, Y.; Meyer, H. M.; Cummings, P. T.; Gogotsi, Y. Influence of Surface Oxidation on Ion Dynamics and Capacitance in Porous and Nonporous Carbon Electrodes. *J. Phys. Chem. C* **2016**, *120*, 8730−8741.
(36) Dyatkin, B.; Mamontov, E.; Cook, K. M.; Gogotsi, Y. Capacitance, Charge Dynamics, and Electrolyte-Surface Interactions in Functionalized Carbide-Derived Carbon Electrodes. *Prog. Nat. Sci.: Mater. Int.* **2015**, *25*, 631−641.
(37) Niedermeyer, H.; Hallett, J. P.; Villar-Garcia, I. J.; Hunt, P. A.; Welton, T. Mixtures of Ionic Liquids. *Chem. Soc. Rev.* **2012**, *41*, 7780−7802.
(38) Mamontov, E.; Herwig, K. W. A Time-of-Flight Backscattering Spectrometer at the Spallation Neutron Source, Basis. *Rev. Sci. Instrum.* **2011**, *82*, 085109.
(39) Bee, M. *Quasielastic Neutron Scattering: Principles and Applications in Solid State Chemistry, Biology, and Materials Science*; Adam Hilger, Bristol, 1998; p 28.
(40) Osti, N. C.; Coté, A.; Mamontov, E.; Ramirez-Cuesta, A.; Wesolowski, D. J.; Diallo, S. O. Characteristic Features of Water Dynamics in Restricted Geometries Investigated with Quasi-Elastic Neutron Scattering. *Chem. Phys.* **2016**, *465*, 1−8.
(41) Osti, N. C.; Naguib, M.; Ostadhossein, A.; Xie, Y.; Kent, P. R. C.; Dyatkin, B.; Rother, G.; Heller, W. T.; van Duin, A. C. T.; Gogotsi, Y.; Mamontov, E. Effect of Metal Ion Intercalation on the Structure of Mxene and Water Dynamics on Its Internal Surfaces. *ACS Appl. Mater. Interfaces* **2016**, *8*, 8859−8863.
(42) Aoun, B.; González, M. A.; Ollivier, J.; Russina, M.; Izaola, Z.; Price, D. L.; Saboungi, M. L. Translational and Reorientational Dynamics of an Imidazolium-Based Ionic Liquid. *J. Phys. Chem. Lett.* **2010**, *1*, 2503−2507.
(43) Mahurin, S. M.; Mamontov, E.; Thompson, M. W.; Zhang, P.; Turner, C. H.; Cummings, P. T.; Dai, S. Relationship between Pore Size and Reversible and Irreversible Immobilization of Ionic Liquid Electrolytes in Porous Carbon under Applied Electric Potential. *Appl. Phys. Lett.* **2016**, *109*, 143111.
(44) Chathoth, S. M.; Mamontov, E.; Dai, S.; Wang, X.; Fulvio, P. F.; Wesolowski, D. J. Fast Diffusion in a Room Temperature Ionic Liquid Confined in Mesoporous Carbon. *Europhys. Lett.* **2012**, *97*, 66004.
(45) Chathoth, S. M.; Mamontov, E.; Fulvio, P. F.; Wang, X.; Baker, G. A.; Dai, S.; Wesolowski, D. J. An Unusual Slowdown of Fast Diffusion in a Room Temperature Ionic Liquid Confined in Mesoporous Carbon. *Europhys. Lett.* **2013**, *102*, 16004.
(46) Singwi, K. S.; Sjölander, A. Diffusive Motions in Water and Cold Neutron Scattering. *Phys. Rev.* **1960**, *119*, 863−871.
(47) Richey, F. W.; Dyatkin, B.; Gogotsi, Y.; Elabd, Y. A. Ion Dynamics in Porous Carbon Electrodes in Supercapacitors Using in Situ Infrared Spectroelectrochemistry. *J. Am. Chem. Soc.* **2013**, *135*, 12818−12826.

DOI: 10.1021/acs.jpcc.8b02521
J. Phys. Chem. C 2018, 122, 10476−10481